AE4304P: Stochastic Aerospace Systems Practical

Analysis of asymmetrical aircraft responses for a rigid aircraft in asymmetrical atmospheric turbulence conditions

Friday 18th October, 2024

by

Bo Lee 5225604

Version Control			
Version	**Date**	**Author(s)**	**Description**
1.0		All	First Hand-in

Teachers: Prof. Dr. Ir. M. Mulder
Tutor: Prof. Dr. Ir. M. Mulder
Faculty: Faculty of Aerospace Engineering, Delft

Cover: None
Style: TU Delft Report Style, with modifications by Daan Zwaneveld and Tim Dammerman.

Contents

1 Introduction

Atmospheric turbulence is a source of stochastic perturbance on rigid-body aircraft which affects the aircraft's motion in both symmetric and asymmetric maneuvers. Turbulent air itself is produced by several environmental factors in the atmosphere such as temperature gradients, wind shear, clouds and mountains. Each of these factors plays a different role depending on an aircraft's location in the atmosphere however the net effect is an overall more negative flying experience. Turbulence increases the instability of the aircraft due to sudden gusts which in turn increases pilot fatigue and decreases passenger comfort.

This report analyzes the effect of asymmetric atmospheric turbulence on asymmetrical aircraft responses for a Cessna Ce500 Citation I [1]. The effects are analyzed for two turbulence conditions separately, firstly for horizontal turbulence:

- $L_g = 150$ m
- $\sigma_{u_g} = 3$ m/s

And secondly for vertical turbulence:

- $L_g = 150$ m
- $\sigma_{w_g} = 2$ m/s

These two conditions will induce different responses in the flight of an aircraft and therefore it is useful to separate them to investigate their individual effects. To analyze the aircraft's response to these conditions four main assumptions and simplifications must be made. These assumptions [1] are:

1. Atmospheric turbulence is a random process with Gaussian distribution
2. Atmospheric turbulence is a stationary process
3. Atmospheric turbulence is homogenous along the flight path
4. Atmospheric turbulence is an isotropic process

The analyses enabled by these assumptions give insight into the stochastic processes behind turbulence. It also allows for the comparison of both turbulence conditions as aircraft responses can be calculated separately in the analysis stages. This is important as investigation into the aircraft's response to different conditions can reveal key characteristics about its flight envelope.

Chapter 2 details the creation of the aircraft model and the design of a stabilising controller and following a time domain analysis is performed in chapter 3. This information is then used to perform a spectral analysis in chapter 4 with details on variances given in chapter 5. Finally, a conclusion on the findings is given in chapter 6.

2 Stability Analysis

To analyze the stability of asymmetric motions in response to turbulence the aircraft equations of motion are set up in state-space form as shown in equation (2.1).

$$\dot{x}(t) = Ax(t) + Bu(t) \tag{2.1}$$

Where A is the 10x10 state matrix given by equation (2.2), x is the 1x10 state vector given by equation (2.3), B is the 10x5 input matrix given by equation (2.4) and u 1x5 is the input vector given by equation (2.5).

$$A = \begin{bmatrix} y_\beta & y_\varphi & y_p & y_r & 0 & 0 & 0 & 0 & y_{\beta g} & 0 \\ 0 & 0 & 2\frac{V}{b} & 0 & 0 & 0 & 0 & 0 & 0 & 0 \\ l_\beta & 0 & l_p & l_r & l_{u_g} & 0 & l_{\alpha_g} & 0 & l_{\beta_g} & 0 \\ n_\beta & 0 & n_p & n_r & n_{u_g} & 0 & n_{\alpha_g} & 0 & n_{\beta_g} & 0 \\ 0 & 0 & 0 & 0 & 0 & 1 & 0 & 0 & 0 & 0 \\ 0 & 0 & 0 & 0 & -\left(\frac{V}{L_g}\right)^2 \frac{1}{\tau_1\tau_2} & -\frac{\tau_1+\tau_2}{\tau_1\tau_2}\left(\frac{V}{L_g}\right) & 0 & 0 & 0 & 0 \\ 0 & 0 & 0 & 0 & 0 & 0 & 0 & 1 & 0 & 0 \\ 0 & 0 & 0 & 0 & 0 & 0 & -\left(\frac{V}{L_g}\right)^2 \frac{1}{\tau_4\tau_5} & -\frac{\tau_4+\tau_5}{\tau_4\tau_5}\left(\frac{V}{L_g}\right) & 0 & 0 \\ 0 & 0 & 0 & 0 & 0 & 0 & 0 & 0 & 0 & 1 \\ 0 & 0 & 0 & 0 & 0 & 0 & 0 & 0 & -\left(\frac{V}{L_g}\right)^2 & -2\frac{V}{L_g} \end{bmatrix} \tag{2.2}$$

$$x = \begin{bmatrix} \beta & \varphi & \frac{pb}{2V} & \frac{rb}{2V} & \hat{u}_g & \hat{u}_g^* & \alpha_g & \alpha_g^* & \beta_g & \beta_g^* \end{bmatrix} \tag{2.3}$$

$$B = \begin{bmatrix} 0 & y_{\delta_r} & 0 & 0 & 0 \\ 0 & 0 & 0 & 0 & 0 \\ l_{\delta_a} & l_{\delta_r} & 0 & 0 & 0 \\ n_{\delta_a} & n_{\delta_r} & 0 & 0 & 0 \\ 0 & 0 & \frac{\tau_3}{\tau_1\tau_2}\sqrt{\frac{V}{L_g} I_{\hat{u}_g}(0,B)} & 0 & 0 \\ 0 & 0 & \left(1-\frac{\tau_3(\tau_1+\tau_2)}{\tau_1\tau_2}\right)\frac{1}{\tau_1\tau_2}\sqrt{\left(\frac{V}{L_g}\right)^3 I_{\hat{u}_g}(0,B)} & 0 & 0 \\ 0 & 0 & 0 & \frac{\tau_6}{\tau_4\tau_5}\sqrt{\frac{V}{L_g} I_{\alpha g}(0,B)} & 0 \\ 0 & 0 & 0 & \left(1-\frac{\tau_6(\tau_4+\tau_5)}{\tau_4\tau_5}\right)\frac{1}{\tau_4\tau_5}\sqrt{\left(\frac{V}{L_g}\right)^3 I_{\alpha g}(0,B)} & 0 \\ 0 & 0 & 0 & 0 & \sigma_{\beta_g}\sqrt{\frac{3V}{L_g}} \\ 0 & 0 & 0 & 0 & (1-2\sqrt{3})\sigma_{\beta_g}\sqrt{\left(\frac{V}{L_g}\right)^3} \end{bmatrix} \tag{2.4}$$

$$u = \begin{bmatrix} \delta_a & \delta_r & w_1 & w_2 & w_3 \end{bmatrix} \tag{2.5}$$

With the given flight conditions inputted the matrices A and B provide the results given in equation (2.6) and equation (2.7) respectively.

$$A = \begin{bmatrix} -0.317 & 0.242 & -0.0308 & -27.1 & 0 & 0 & 0 & 0 & -0.317 & 0 \\ 0 & 0 & 27.2 & 0 & 0 & 0 & 0 & 0 & 0 & 0 \\ -0.940 & 0 & -3.58 & 1.19 & -0.878 & 0 & -2.86 & 0 & -0.940 & 0 \\ 0.485 & 0 & -0.155 & -0.490 & 0.0635 & 0 & -0.120 & 0 & 0.485 & 0 \\ 0 & 0 & 0 & 0 & 0 & 1 & 0 & 0 & 0 & 0 \\ 0 & 0 & 0 & 0 & -26.8 & -14.4 & 0 & 0 & 0 & 0 \\ 0 & 0 & 0 & 0 & 0 & 0 & 0 & 1 & 0 & 0 \\ 0 & 0 & 0 & 0 & 0 & 0 & -74.4 & -23.9 & 0 & 0 \\ 0 & 0 & 0 & 0 & 0 & 0 & 0 & 0 & 0 & 1 \\ 0 & 0 & 0 & 0 & 0 & 0 & 0 & 0 & -1.47 & -2.43 \end{bmatrix} \tag{2.6}$$

$$B = \begin{bmatrix} 0 & 0.0646 & 0 & 0 & 0 \\ 0 & 0 & 0 & 0 & 0 \\ -1.74 & 0.331 & 0 & 0 & 0 \\ -0.0850 & -0.345 & 0 & 0 & 0 \\ 0 & 0 & 0.0217 & 0 & 0 \\ 0 & 0 & -0.250 & 0 & 0 \\ 0 & 0 & 0 & 0.0185 & 0 \\ 0 & 0 & 0 & -0.343 & 0 \\ 0 & 0 & 0 & 0 & 0.0210 \\ 0 & 0 & 0 & 0 & -0.0362 \end{bmatrix} \tag{2.7}$$

These equations provide the basis for aircraft state calculations and full state-space simulation can be performed with the output equation given in equation (2.8).

$$y(t) = Cx(t) + Du(t) \tag{2.8}$$

Since information is required for all states the output matrix, C, becomes a 10x10 identity matrix. Additionally, as the outputs depend only on the state variables the feedthrough matrix, D, becomes a zero matrix.

Now with the full state-space model, it is possible to analyse the stability of the open-loop, uncontrolled asymmetric eigenmotions. This analysis is performed using pole-zero maps and checking for eigenvalues in the open right-half plane to indicate instability. The pole-zero map for the uncontrolled full aircraft model is given in figure 2.1 and its corresponding eigenvalues in table 2.1.

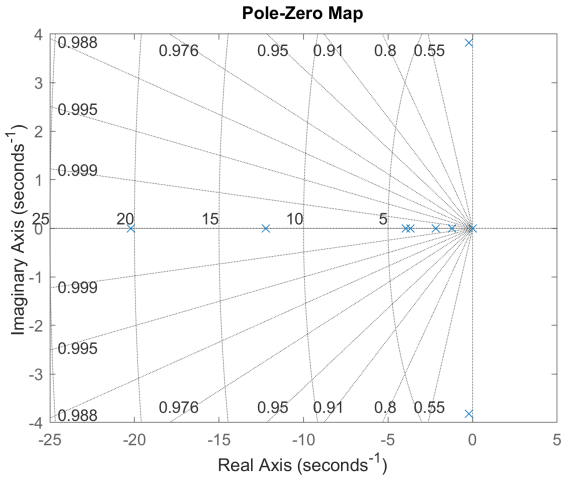

Figure 2.1: Full system

Table 2.1: Full uncontrolled system eigenvalues

Full		**Eigenmode**
Real	**Imaginary**	**Type**
-0.2209	+3.8254i	Dutch roll
-0.2209	+3.8254i	Dutch roll
-3.9571	0.0000i	Roll
+0.0134	0.0000i	Spiral (unstable)

It can be seen that one eigenvalue for the model sits in the open right-half plane with a value of +0.0134. The remaining eigenvalues are all stable. The periodic eigenvalues, those with both real and imaginary values, are assumed to represent the Dutch roll eigenmode. The highly damped eigenvalue is assumed to represent the roll eigenmode due to its characteristically high damping. The final eigenvalue is most likely the eigenvalue relating to the spiral eigenmode which in some aircraft can be unstable. In this case, full stability is preferred therefore the design of a roll-damper is required. It is possible to use the roll-damper equation given in equation (2.9).

$$\delta_a = K_\varphi \varphi + K_p p \tag{2.9}$$

Taking an initial value for K_φ as -0.1 and leaving K_p as 0 provides satisfactory stability for the system. This is shown by the pole-zero map in figure 2.2 and eigenvalues given in table 2.2.

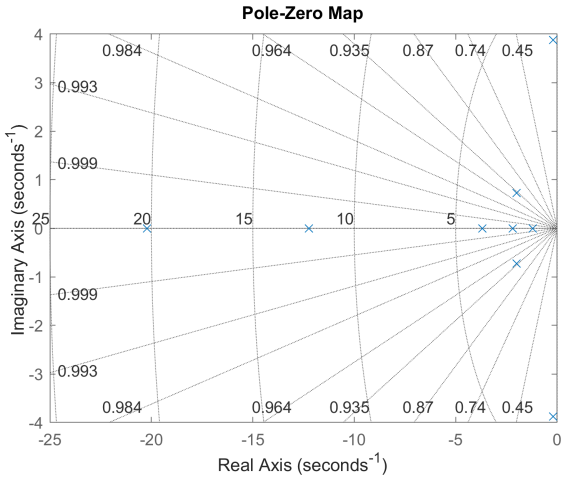

Figure 2.2: Full controlled system pole-zero map

Table 2.2: Full controlled system eigenvalues

Closed loop		**Eigenmode**
Real	**Imaginary**	**Type**
-0.1900	+3.8738i	Dutch roll
-0.1900	-3.8738i	Dutch roll
-2.0027	+0.7272i	Roll
-2.0027	-0.7272i	Roll
-2.1870	0.0000i	Spiral

The spiral eigenmode has been stabilised at the cost of periodicity in the roll eigenmode. This is a negative change in roll stability however its damping is still high and the periodicity is relatively low. Therefore this change will be deemed acceptable, thus going forward the controlled full model will be used both for the time domain analysis and the spectral analysis in both turbulence conditions.

3 Time-Domain Analysis

To begin the stochastic analysis of the aircraft models measurement data must be generated through time-domain simulations. The response of four asymmetric flight states (β, φ, $\frac{pb}{2V}$, $\frac{rb}{2V}$) is simulated from the full model for both turbulence conditions. Additionally, for both conditions lateral acceleration, a_y, is also simulated. This is calculated with the formula given in equation (3.1).

$$a_y = \frac{d}{dt} V sin(\beta + \psi) \approx V(\dot{\beta} + \dot{\psi}) \tag{3.1}$$

Calculating lateral acceleration can be done directly from the system states. The variables $\dot{\beta}$ and $\dot{\psi}$ can be found individually using equation (3.2) and equation (3.3).

$$\dot{\beta} = \beta y_\beta + \varphi y_\varphi + \frac{pb}{2V} y_p + \beta_g y_{\beta_g} + \frac{rb}{2V} y_r \tag{3.2}$$

$$\dot{\psi} \approx r = \frac{2V}{b} \frac{rb}{2V} \tag{3.3}$$

These equations can then be substituted into equation (3.1) to get equation (3.4).

$$a_y = V \left(\beta y_\beta + \varphi y_\varphi + \frac{pb}{2V} y_p + \beta_g y_{\beta_g} + \frac{rb}{2V} \left(\frac{2V}{b} + y_r \right) \right) \tag{3.4}$$

Finally, the new 5x10 output matrix, C, can be formed. This is given in equation (3.5).

$$C = \begin{bmatrix} 1 & 0 & 0 & 0 & 0 & 0 & 0 & 0 & 0 & 0 \\ 0 & 1 & 0 & 0 & 0 & 0 & 0 & 0 & 0 & 0 \\ 0 & 0 & 1 & 0 & 0 & 0 & 0 & 0 & 0 & 0 \\ 0 & 0 & 0 & 1 & 0 & 0 & 0 & 0 & 0 & 0 \\ Vy_b & Vy_\varphi & Vy_p & V\left(\frac{2V}{b} + y_r\right) & 0 & 0 & 0 & 0 & Vy_{\beta_g} & 0 \end{bmatrix} \tag{3.5}$$

To incorporate turbulence into the system input vectors are created for the horizontal, u_g, and vertical turbulence, w_g. Therefore, the two new input vectors are given by u_u (equation (3.6)) and u_w (equation (3.7)).

$$u_u = \begin{bmatrix} 0 & 0 & u_g & 0 & 0 \end{bmatrix} \tag{3.6}$$

$$u_w = \begin{bmatrix} 0 & 0 & 0 & w_g & 0 \end{bmatrix} \tag{3.7}$$

As the aircraft simulation is performed in discrete time, the size of the u vectors is based on the length of the simulation and time interval. In this case, a time of 60 s and interval of 0.01 s is taken making the u vectors 5x6001.

The resulting simulation responses for the model are shown in figure 3.1, figure 3.2, figure 3.3, figure 3.4, figure 3.5, and figure 3.6 for both turbulence conditions.

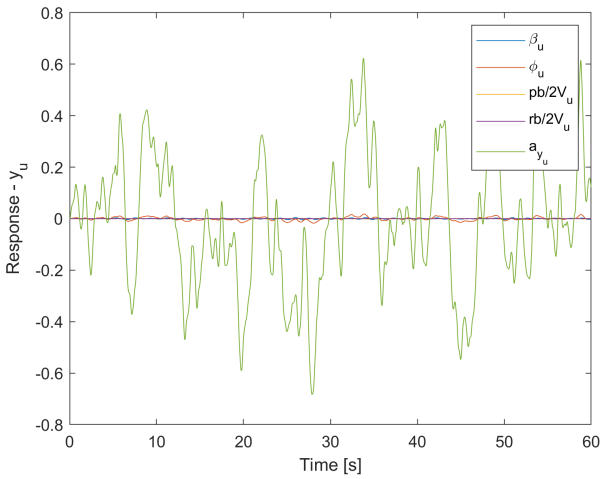

(a) Output response (y_u)

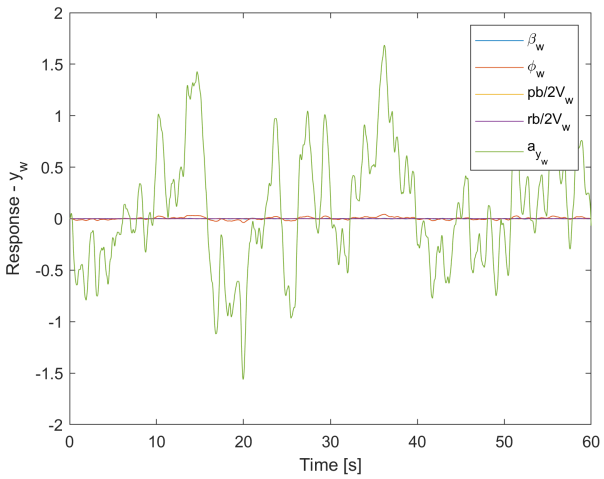

(b) Output response (y_w)

Figure 3.1: Output response for turbulence conditions u_u (equation (3.6)) and u_w (equation (3.7))

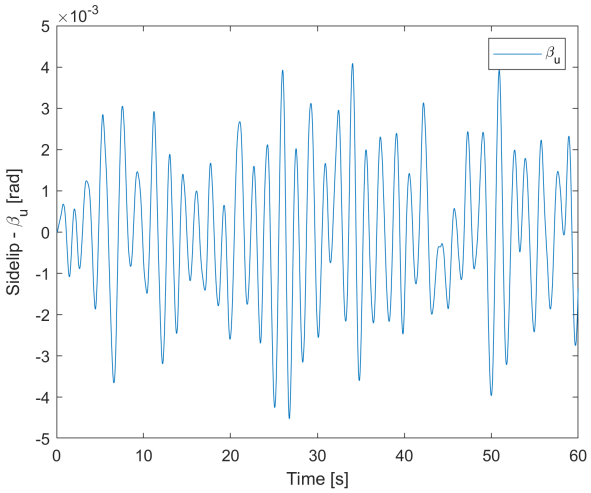

(a) Sideslip (β_u)

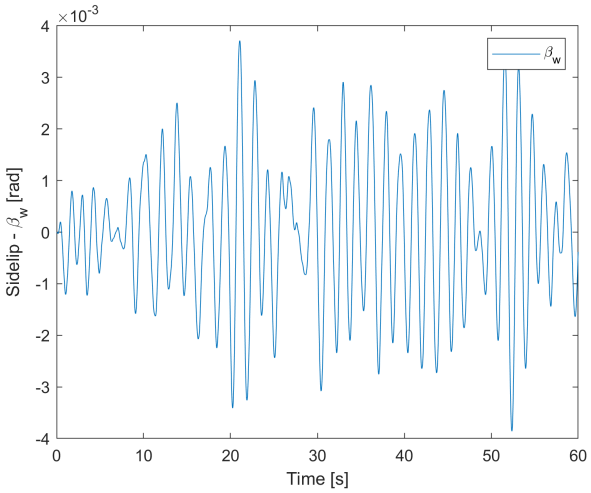

(b) Sideslip (β_w)

Figure 3.2: Sideslip response for turbulence conditions u_u (equation (3.6)) and u_w (equation (3.7))

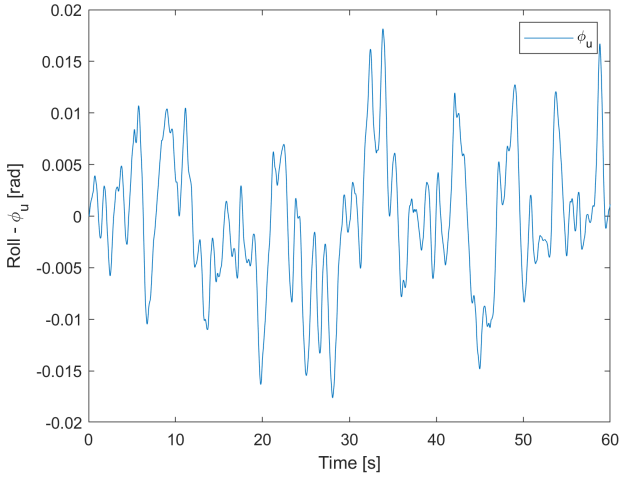

(a) Roll (φ_u)

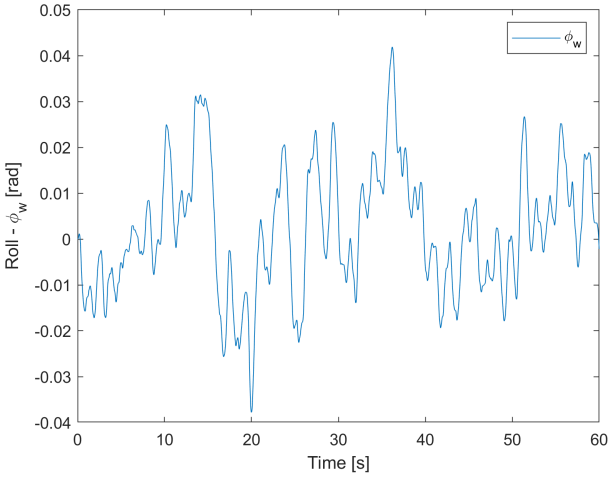

(b) Roll (φ_w)

Figure 3.3: Roll response for turbulence conditions u_u (equation (3.6)) and u_w (equation (3.7))

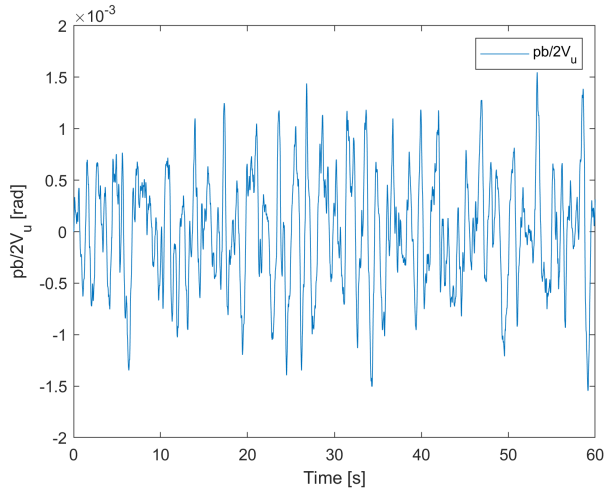

(a) Roll rate ($\frac{pb}{2V}_u$)

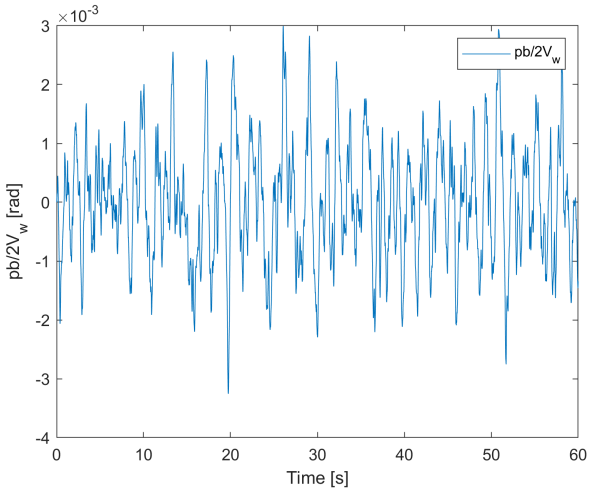

(b) Roll rate ($\frac{pb}{2V}_w$)

Figure 3.4: Roll rate response for turbulence conditions u_u (equation (3.6)) and u_w (equation (3.7))

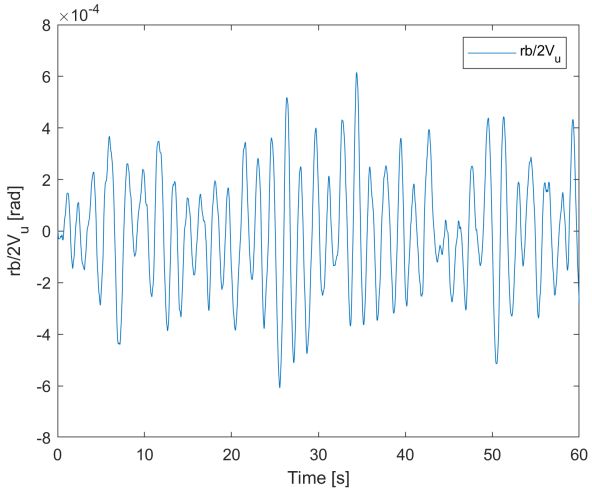

(a) Yaw rate ($\frac{rb}{2V}_u$)

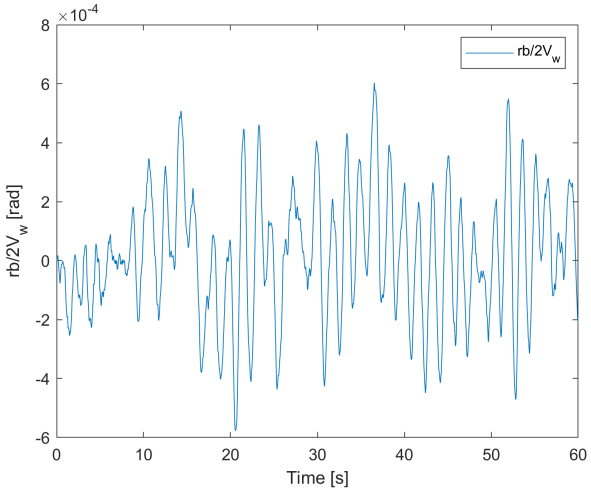

(b) Yaw rate ($\frac{rb}{2V}_w$)

Figure 3.5: Yaw rate response for turbulence conditions u_u (equation (3.6)) and u_w (equation (3.7))

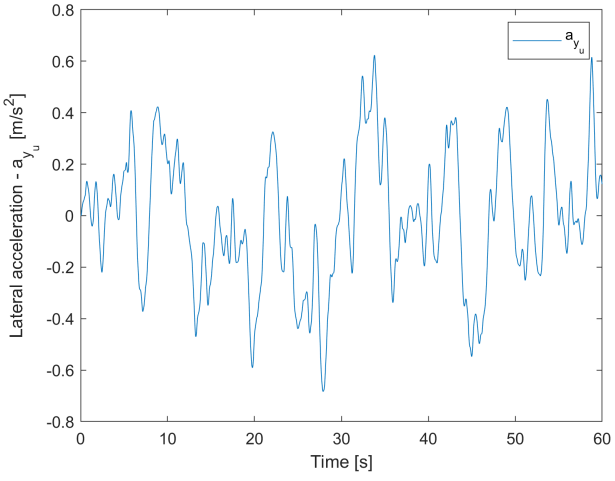

(a) Lateral acceleration (a_{y_u})

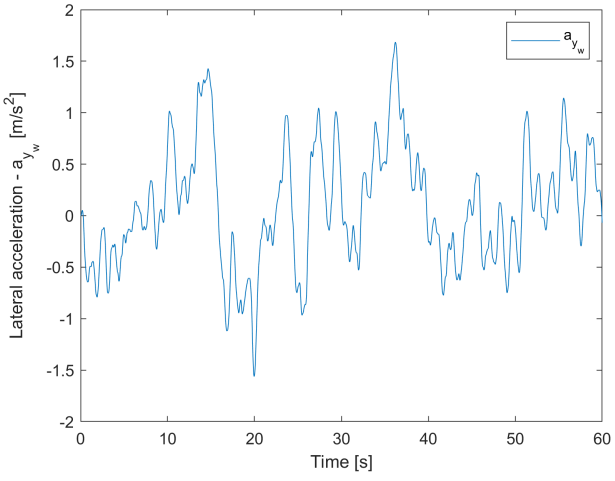

(b) Lateral acceleration (a_{y_w})

Figure 3.6: Lateral acceleration response for turbulence conditions u_u (equation (3.6)) and u_w (equation (3.7))

4 Spectral Analysis

With time series data acquired, stochastic analysis of the data can begin. This is done to compare the results of different power spectral density (PSD) functions and see their advantages and disadvantages. Thus the spectral analysis is performed with an analytical PSD, experimental PSD and a smoothed experimental PSD. The analytical PSD is calculated using equation (4.1).

$$S_{\bar{x}\bar{x}} = \lim_{T\to\infty} \frac{1}{2T} |\bar{A}(\omega)|^2 \tag{4.1}$$

Where T is the sampled period and $\bar{A}(\omega)$ is the frequency magnitude. Functionally this is done by finding the bode values of the states for both the horizontal and vertical turbulence and squaring the result.

The experimental method starts by finding the periodogram of each state by calculating their discrete Fourier transforms and scaling that with the time interval. The calculation of the Fourier transforms is done in MATLAB using the "fft.m" function. A PSD estimate is then found using equation (4.2).

$$I_{Nxx}[k] = \frac{\Delta t}{N} |\bar{X}[k]|^2 \tag{4.2}$$

Where N is the number of samples and $\bar{X}[k]$ is the Fourier transform of the time-series data. Finally, the smoothed experimental is found by applying a smoothing filter given in equation (4.3), equation (4.4) and equation (4.5).

$$\Phi_{\text{estimate}}[1] = 0.5\Phi[1] + 0.5\Phi[2] \tag{4.3}$$

$$\Phi_{\text{estimate}}[k] = 0.25\Phi[k-1] + 0.5\Phi[k] + 0.25\Phi[k+1] \tag{4.4}$$

$$\Phi_{\text{estimate}}[N] = 0.5\Phi[N-1] + 0.5\Phi[N] \tag{4.5}$$

This can be done simply by convoluting a smoothing matrix over the experimental PSD data. This matrix is given in equation (4.6) for filter f.

$$f = \begin{bmatrix} 0.25 & 0.5 & 0.25 \end{bmatrix} \tag{4.6}$$

The results for all three methods in both turbulence conditions are given in figure 4.1, figure 4.2, figure 4.3, figure 4.4 and figure 4.5.

These PSDs give an insight into the differences in aircraft response for each turbulence condition. It can be seen that the spectral responses for the vertical turbulence condition, u_w, exhibit equivalent or higher peak power than those of the horizontal turbulence condition, u_u. Also, the overall power of the vertical turbulence condition is generally higher which shows a more damped response in horizontal turbulence conditions. The frequencies at which the peak occurs over both conditions are overall the same at around 3 rad/s. It is interesting to note that the horizontal turbulence condition often exhibits a dip in power before its peak. This shows that the aircraft damps its response even further before its peak frequency in horizontal turbulence conditions.

Certain eigenmodes can also be related to the PSD graphs by comparing the frequencies of the periodic eigenmodes and the peaks of the PSDs. The highest peaks can be seen in figure 4.3 which relate these graphs to the Dutch roll eigenmode which has the highest periodicity. The second-highest peaks can be seen in figure 4.2 which would relate these to the roll eigenmode as it exhibits slight periodicity after introducing the roll damper. The spiral eigenmode is heavily damped with little periodicity so it is most likely related to figure 4.5 due to its low overall power.

The 3 methods used to find these PSDs all result in similar graphs. Both periodograms follow the analytical response for the most part except with slight deviations at high frequencies primarily in figure 4.2 and figure 4.5. This may be caused by the windowing effect when calculating the discrete Fourier transform causing spectral leakages due to the window being too short to encompass the entire period. Overall however the experimental periodograms show acceptable mapping of the PSD with the smoothed periodogram being preferable due to its large noise reduction. A stronger filter could have been used to further damp out the noise, especially at high frequencies.

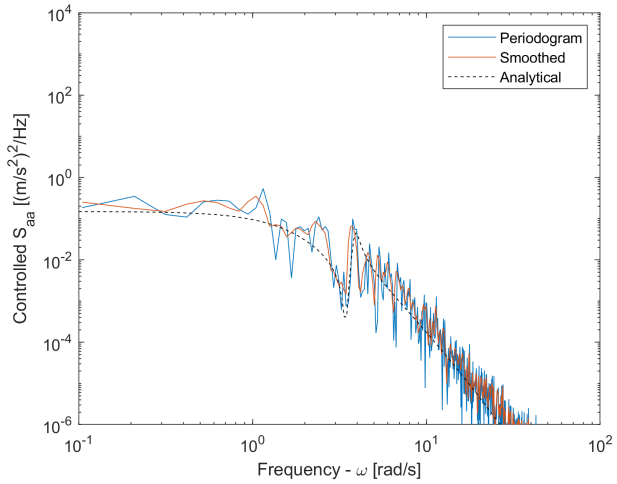

(a) Lateral acceleration for u_u (equation (3.6))

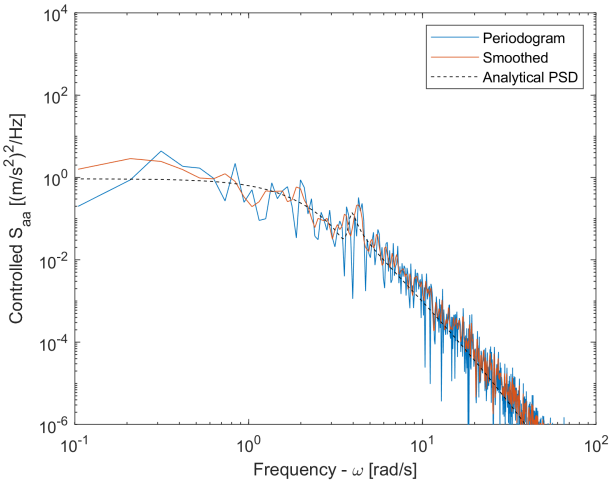

(b) Lateral acceleration for u_w (equation (3.7))

Figure 4.1: PSDs of lateral acceleration

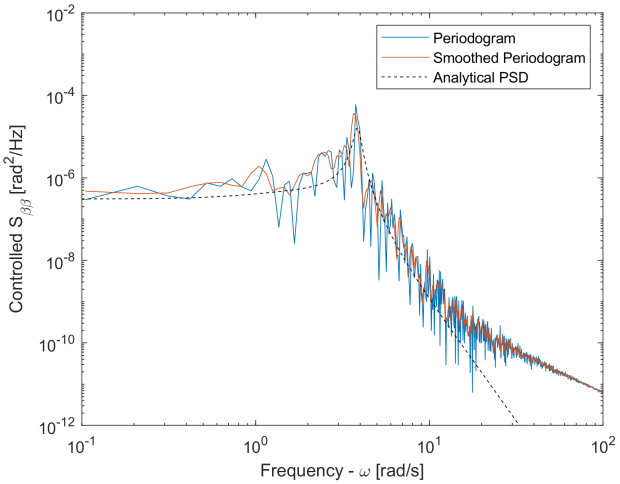

(a) Side slip for u_u (equation (3.6))

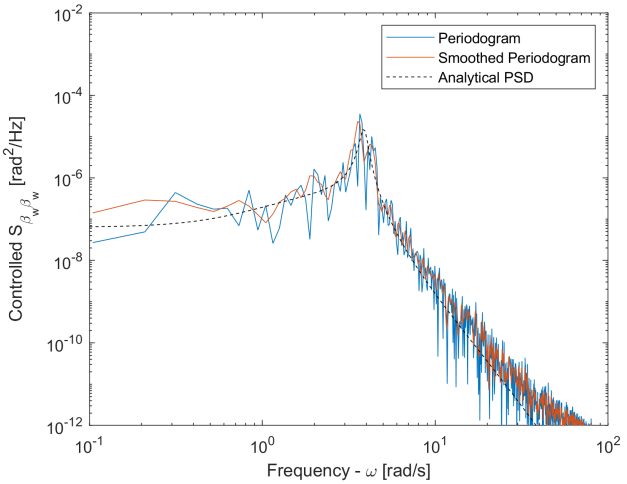

(b) Side slip for u_w (equation (3.7))

Figure 4.2: PSDs of side slip

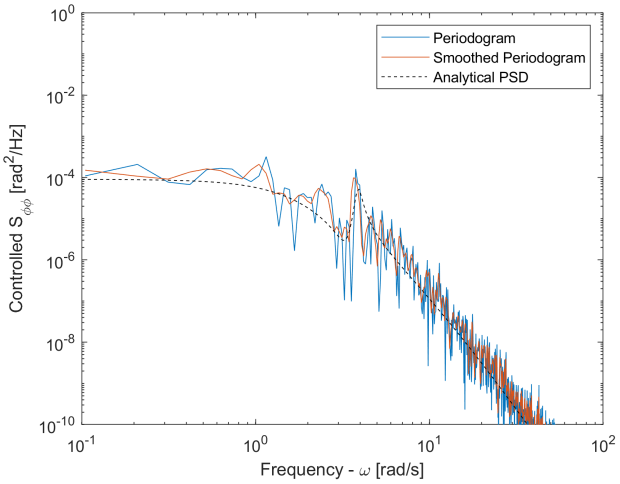

(a) Roll for u_u (equation (3.6))

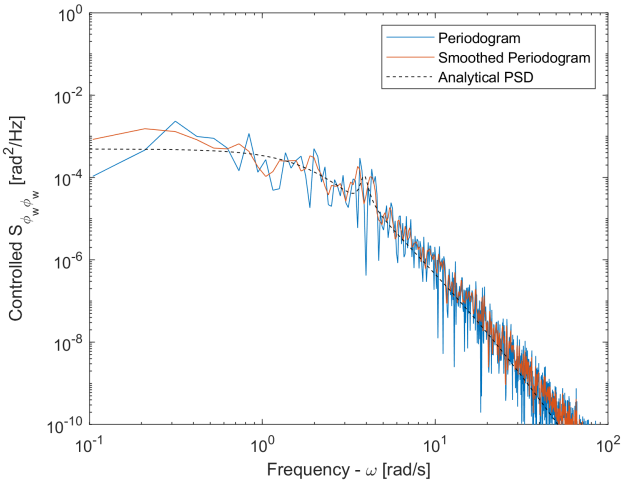

(b) Roll for u_w (equation (3.7))

Figure 4.3: PSDs of roll

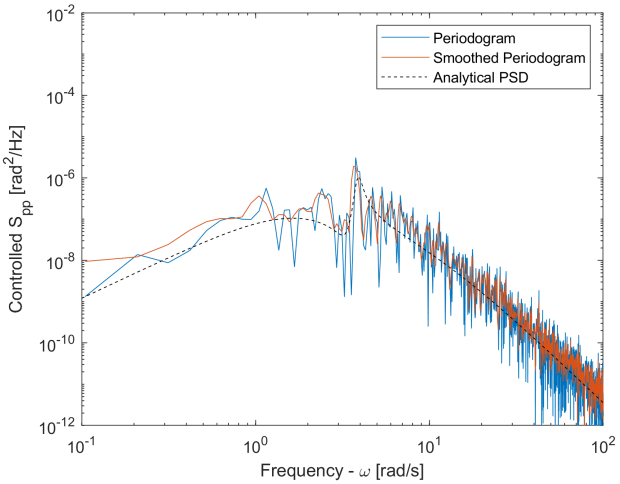

(a) Roll rate for u_u (equation (3.6))

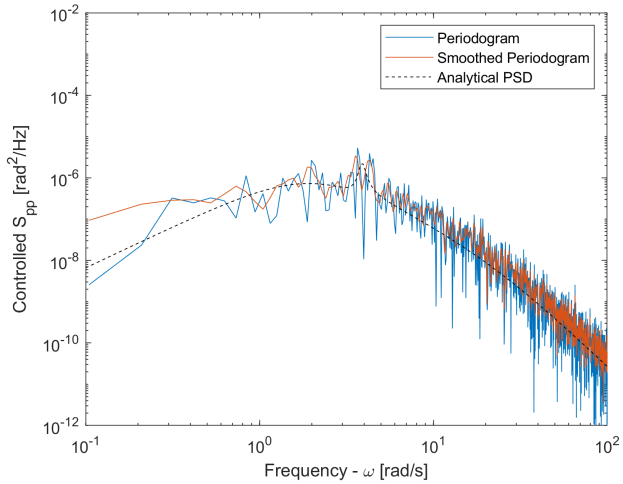

(b) Roll rate for u_w (equation (3.7))

Figure 4.4: PSDs of roll rate

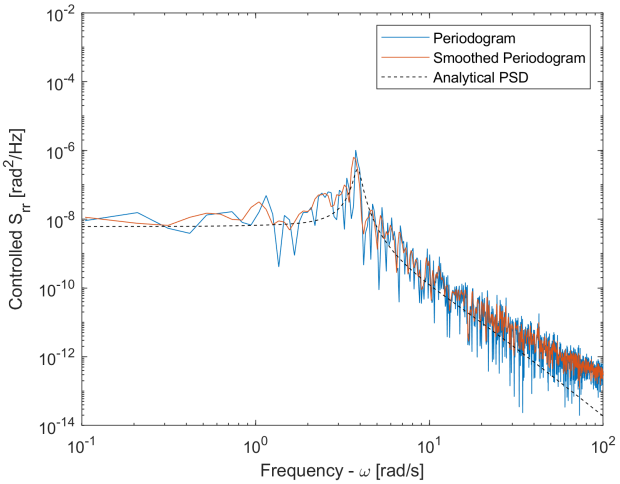

(a) Yaw rate for u_u (equation (3.6))

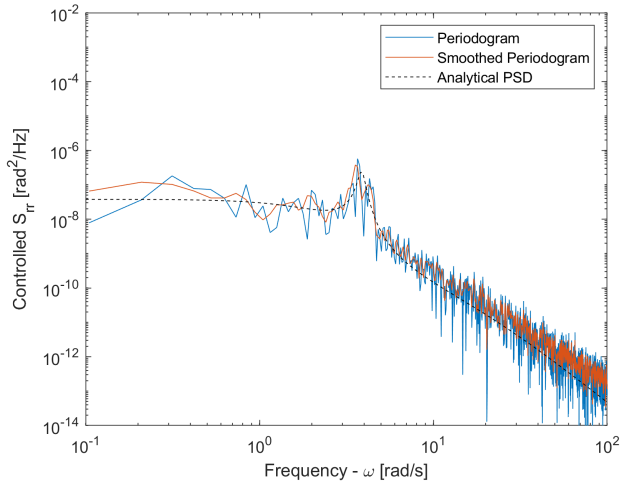

(b) Yaw rate for u_w (equation (3.7))

Figure 4.5: PSDs of yaw rate

5 Variances

Finally, the variances of all the states and lateral acceleration are calculated for both turbulence conditions. The variances are found from the analytical and experimental PSDs as well as the time-series data using the MATLAB "var.m" function. The calculation of variance for the analytical and experimental power spectra can be done by simply integrating and scaling the results of the PSDs, S_{xx}, this is shown in equation (5.1).

$$\sigma_x^2 = \frac{1}{\pi} \int_0^\infty S_{xx}(\omega) d\omega \tag{5.1}$$

The MATLAB "var.m" function uses a different method that finds the average of the sum of differences between a specific value and the total average. This is shown in equation (5.2).

$$\sigma_x^2 = \frac{1}{N-1} \sum_{i=1}^{N} |X_i - \mu_x|^2 \tag{5.2}$$

The variances found using each method are shown for both turbulence conditions in table 5.1 and table 5.2.

Table 5.1: Variances of the model for u_u (equation (3.6))

Method	β [rad^2]	φ [rad^2]	$\frac{pb}{2V}$ [rad^2]	$\frac{rb}{2V}$ [rad^2]	a_y [m^2/s^4]
Analytical	3.4600e-06	5.0592e-05	3.7474e-07	5.9955e-08	7.5900e-2
Experimental	5.7729e-06	8.7632e-05	6.1437e-07	9.7388e-08	1.3270e-1
Experimental Smoothed	5.7676e-06	8.6312e-05	6.1435e-07	9.7299e-08	1.3050e-1
var.m Function	2.8846e-06	4.3542e-05	3.0718e-07	4.8685e-08	6.5900e-2

Table 5.2: Variances of the model for u_w (equation (3.7))

Method	β [rad^2]	φ [rad^2]	$\frac{pb}{2V}$ [rad^2]	$\frac{rb}{2V}$ [rad^2]	a_y [m^2/s^4]
Analytical	3.0813e-06	2.7376e-04	1.4045e-06	6.9405e-08	4.8970e-1
Experimental	4.0661e-06	3.9239e-04	2.0422e-06	9.3963e-08	7.0620e-1
Experimental Smoothed	4.0649e-06	3.7932e-04	2.0422e-06	9.2931e-08	6.8140e-1
var.m Function	2.0324e-06	1.8807e-04	1.0211e-06	4.6337e-08	3.3770e-1

Analysing the variances, it can be seen for both conditions that there is roughly a factor of 2 difference between the MATLAB "var.m" variances and the variances found from the experimental spectra. This is likely because the "var.m" function samples directly from the time domain compared to the spectra integration method which samples from the frequency domain. Because the integration method is based in the frequency domain it benefits from a longer signal duration which can improve its accuracy. A similar difference can be seen between the analytical and experimental variances as the analytical variances are roughly a factor of 1.5 smaller. These differences arise mainly due to the greater noise in the experimental periodograms resulting in more variance. This also explains the reason why the smoothed experimental periodogram has a slightly lower variance than the standard experimental periodogram. General differences between all methods may also arise due to the high-frequency

inconsistencies in the PSDs. Using better windowing functions may reduce the differences in variance by mitigating transient effects.

The variances for the horizontal turbulence condition are mostly higher than those of the vertical turbulence condition. This could be an effect of the higher horizontal turbulence compared to the vertical turbulence which results in a broader energy spectrum and thus greater differences across frequencies. This excludes the lateral acceleration variances which are a factor of 5 greater in the vertical turbulence condition. The explanation here is clear as vertical turbulence will have a much greater influence on the lateral acceleration than horizontal turbulence. This results in more power and thus more variance in this response.

6 Conclusion

To gain deeper insight into the effect of atmospheric turbulence on asymmetrical aircraft responses arising from both horizontal and vertical turbulence this report has shown the result of multiple stochastic analyses. All analyses were performed on a Cessna Ce500 Citation I aircraft model for both turbulence conditions separately, to compare the response of the aircraft in different conditions. The uncontrolled aircraft model was found to be unstable for the spiral eigenmode, however, stability was achieved by introducing a roll damper. This however was at the cost of introducing periodicity into the roll eigenmode. While this is a negative trade-off in terms of roll stability the aircraft is still controllable overall and therefore the model with the roll damper is preferable to the uncontrolled aircraft model.

Spectral analysis was performed with both analytical and experimental methods. The analytical power spectral density (PSD) functions were generated using the frequency magnitude while the experimental PSD functions were found by generating periodograms of each state and then finding the PSD estimate. One experimental PSD was smoothed using a convolution filter which provided less noise results.. The smoothed result was still noisy however and a stronger filter could have been used. Both the analytical and experimental produced comparable PSDs with some inconsistencies at higher frequencies. This occurred due to the windowing effect in the calculating of the discrete Fourier transform (DFT). For higher frequencies in the side slip PSD in the horizontal turbulence condition this produced notable differences. If analysis is required at high frequencies then the calculation of the DFT should be altered or the analytical PSD should be used regarding accuracy. However, for most of the PSDs, the results are valid and can be used to analyse the aircraft responses under turbulence with the smoothed periodogram preferred due to its low noise. These PSDs can also be used to analyse the eigenmodes as each graph also corresponds to a respective eigenmode.

Finally, the variances were calculated from the PSDs and time-series data using the "var.m" function. It was found that there was a factor of 2 difference between the "var.m" method and the integrated experimental periodograms variances. This was due to the differences in calculating variance using time-series data and frequency data. In this case, the PSD-based variances were preferred due to their longer signal durations. This resulted in a more accurate variance that is representative of how variance is distributed across frequencies. However, it is important to note that obtaining the PSD-based variance required the calculation of the PSDs in the first place. Thus if frequency-based variance is not essential and the variance needs to be calculated quickly it is more applicable to use "var.m". Looking at the variances between the turbulence conditions it was found that they were marginally greater for the horizontal turbulence, excluding the lateral acceleration variance. This is due to the stronger turbulence induced in the horizontal condition.

Bibliography

[1] Delft University of Technology. "AE4304P: Stochastic Aerospace Systems Practical". In: *Control Simulation* (Dec. 2023).